Theoretical Analysis of Shear Wave Interference Patterns by Means of Dynamic Acoustic Radiation Forces

Kenneth Hoyt*
Departments of Radiology and Biomedical Engineering,
Comprehensive Cancer Center, University of Alabama at Birmingham,
Birmingham, AL 35294, USA

ABSTRACT

Acoustic radiation forces associated with high intensity focused ultrasound stimulate shear wave propagation allowing shear wave speed and shear viscosity estimation of tissue structures. As wave speeds are meters per second, real time displacement tracking over an extend field-of-view using ultrasound is problematic due to very high frame rate requirements. However, two spatially separated dynamic external sources can stimulate shear wave motion leading to shear wave interference patterns. Advantages are shear waves can be imaged at lower frame rates and local interference pattern spatial properties reflect tissue's viscoelastic properties. Here a theoretical analysis of shear wave interference patterns by means of dynamic acoustic radiation forces is detailed. Using a viscoelastic Green's function analysis, tissue motion due to a pair of focused ultrasound beams and associated radiation forces are presented. Overall, this paper theoretically demonstrates shear wave interference patterns can be stimulated using dynamic acoustic radiation forces and tracked using conventional ultrasound imaging.

1. INTRODUCTION

Physical examination reveals that a fundamental elastic contrast exists between various normal human tissue types [1]. Of clinical importance, many pathological conditions are associated with pronounced changes in the tissue's elastic properties [2-8] that may be monopolized for detection and therapeutic monitoring. It is this impetus that has helped inspire research into the ever expanding biomedical field of tissue elasticity estimation and imaging.

Numerous ultrasound-based methods have been introduced for estimating and visualizing the elastic properties of soft tissue [9-11]. The generalized premise behind these noninvasive techniques is to (1) apply a mechanical stimulus to the target tissue, (2) estimate the deformational response using motion tracking algorithms, and (3) image the displacement-derived elastic property of interest. While first generation tissue elasticity imaging techniques were predominately qualitative in approach and relied on external sources to induce motion, more recent developments have used the acoustic radiation forces associated with focused ultrasound beams to stimulate tissue displacement and shear wave propagation at depth. As radiation force-induced shear wave propagation is intrinsically governed by the viscoelastic properties of the underlying tissues, various quantitative strategies have been proposed for parameter reconstruction [1,12-16].

*Corresponding Author: G082 Volker Hall, 1670 University Blvd, Birmingham, AL 35294-0019 Ph: (205) 934-3116

One particular viscoelastic parameter of interest in biological tissue is the shear wave speed with magnitude on the order of meters per second. Such values can seriously complicate imaging using conventional ultrasound systems as this necessitates frame rates on the order of thousands per second to discretely capture shear wave propagation in real-time. While custom ultrasound scanners can be modified to permit high-frame rate acquisition over an extend field-of-view, such access is typically limited due to proprietary concerns. It is this limitation that led to the development of an imaging method which visualizes slowly moving shear wave interference patterns (termed crawling waves) in real-time using conventional ultrasound technology [17]. Induced using a pair of spatially separated dynamic sources, the main advantage to this imaging method is that spatial properties of the shear wave interference patterns (namely wavelength) reflect local tissue elastic properties [18]. Various image processing strategies have since been proposed for the analysis of shear wave interference patterns and estimation of local viscoelastic parameters [18-21] which have inherent clinical significance.

The initial elasticity imaging system design for inducing shear wave interference patterns used external vibration sources to dynamically induce tissue motion. This configuration is limited to analysis of superficial (or easily accessible) tissues since propagating shear waves are known to be highly attenuated by biological tissues. Given the ability of acoustic radiation forces to stimulate shear wave propagating at tissue depth, it is hypothesized that proper spacing and sequencing of dynamic high intensity acoustic radiation forces coupled with low intensity ultrasound-based displacement tracking algorithms can be used to remotely induce and image shear wave interference patterns. In this paper, a theoretical analysis of shear wave interference patterns by means of dynamic acoustic radiation forces is presented.

2. THEORY

2.1. ACOUSTIC RADIATION FORCE

The physical origin of radiation force exertion by an ultrasound wave on a dissipative medium (such as soft tissue) was described by Torr [22]. In short, momentum transfer from an ultrasound wave to soft tissue results in the application of a body force in the direction of wave propagation. Assuming plane wave conditions, acoustic radiation forces F associated with a focused ultrasound beam in soft tissue can be described by the following equation [23]:

$$F(\vec{r},t)=\frac{2\alpha I(\vec{r},t)}{c_p} \tag{1}$$

where α is the ultrasound absorption coefficient, I the local intensity of the ultrasound beam, c_p is the bulk wave speed in the medium, and t is the time variable The three orthogonal components of the pointing vector $\vec{r}$ are (x_1,x_2,x_3).

2.2. WAVE EQUATIONS OF MOTION

The equations of motion for an isotropic elastic medium can be modeled as follows:

$$\frac{E}{2(1+v)}\nabla^2 u+\frac{E}{2(1+v)(1-2v)}\nabla\nabla\cdot u=\rho\frac{\partial^2 u}{\partial t^2} \tag{2}$$

where E, v, ρ, $\vec{u}$, and t are the Young's modulus, Poisson's ratio, mass density, displacement vector and time variable, respectively. As detailed by Landau and Lifshitz [24], eqn (2) can be split into two decoupled equations of motion that describe either the bulk wave:

$$\frac{\partial^2 u_i}{\partial x^2_i} - \frac{1}{c_p^2}\frac{\partial^2 u_i}{\partial t^2} = 0 \tag{3}$$

or shear wave:

$$\frac{\partial^2 u_j}{\partial x^2_j} - \frac{1}{c_s^2}\frac{\partial^2 u_j}{\partial t^2} = 0 \tag{4}$$

components where c_s is the shear wave speed and x is a spatial variable. Subscripts i and j denote two arbitrary but orthogonal directions. The individual wave speeds introduced in eqns (3) and (4) can be defined as:

$$c_p = \sqrt{\frac{E(1-v)}{\rho(1+v)(1-2v)}} \tag{5}$$

and

$$c_s = \sqrt{\frac{E}{2\rho(1+v)}} \tag{6}$$

Given the shear modulus μ is approximately $E/3$ and assuming a nearly incompressible material ($v = 0.5$), eqn (6) can be further simplified to:

$$c_s = \sqrt{\frac{u}{\rho}} \tag{7}$$

Notwithstanding, biological tissues are known to exhibit shear wave speed dispersion (i.e., dependent on wave frequency) suggesting that a viscoelastic model should be used to more accurately describe the shear elasticity and viscosity components. For a propagating shear wave of frequency F_S, the shear wave speed is described as follows [25]:

$$c_s = \sqrt{\frac{2(\mu^2 + F_s^2\eta_s^2)}{\rho(\mu + \sqrt{\mu^2 + F_s^2\eta_s^2})}} \tag{8}$$

where η_s denotes shear viscosity. As eqn (8) suggests, shear wave speed measurements made over a range of propagation frequencies is one approach to shear modulus and viscosity estimation in soft tissue.

2.3. VISCOELASTIC GREEN'S FUNCTION FORMULATION

Acoustic radiation forces in an infinite, homogeneous medium induce three distinct mechanical waves that propagate away from the focal zone of the ultrasound beam [26-28]. The high frequency bulk wave component propagates instantaneously $(c_p \cong 1540\ \mathrm{m/s})$ whereas the low frequency shear wave component propagates at a much slower speed $(c_s \cong 3\ \mathrm{m/s})$. The third mechanical wave manifests as a coupling term between the bulk and shear components with amplitude less than both. Collectively, these three waves can be accurately modeled using a viscoelastic Green's function formulation [27]:

$$g(\vec{r},t) = g^{p}(\vec{r},t) + g^{s}(\vec{r},t) + g^{ps}(\vec{r},t) \tag{9}$$

where g^p, g^s, and g^{ps} are the pure bulk, shear and coupling terms, respectively. By introducing the viscosity relationships $\upsilon_p = (\eta_p + 2\eta_s)/\rho$ and $\upsilon_s = \eta_s/\rho$ where η_p is bulk viscosity, then the three terms of eqn (9) can be defined in expanded format as:

$$g^{p}(\vec{r},t) = \frac{\gamma^2}{4\pi r\rho c_p\sqrt{2\pi\upsilon_p t}}\exp\left\{\frac{\left(\frac{r}{c_p}-t\right)^2 c_p^2}{2\upsilon_p t}\right\} \tag{10}$$

$$g^{s}(\vec{r},t) = \frac{1-\gamma^2}{4\pi r\rho c_s\sqrt{2\pi\upsilon_s t}}\exp\left\{\frac{\left(\frac{r}{c_s}-t\right)^2 c_s^2}{2\upsilon_s t}\right\} \tag{11}$$

and

$$g^{ps}(\vec{r},t) = \frac{3\gamma^2-1}{4\pi r^3\rho}(I^p - I^s) \tag{12}$$

where

$$I^{p}(\vec{r},t) = \frac{\sqrt{\upsilon_p t}}{\sqrt{2\pi c_p}}\left[\exp\left\{-\frac{t^2c_p^2}{2\upsilon_p t}\right\} - \exp\left\{\frac{\left(\frac{r}{c_p}-t\right)^2 c_p^2}{2\upsilon_p t}\right\}\right] + \frac{t}{2}\left[Erf\left(\frac{c_p t}{\sqrt{2\upsilon_p t}}\right) - Erf\left(\frac{\left(t-\frac{r}{c_p}\right)c_p}{\sqrt{2\upsilon_p t}}\right)\right] \tag{13}$$

and

$$I^{s}(\vec{r},t) = \frac{\sqrt{\upsilon_s t}}{\sqrt{2\pi c_s}}\left[\exp\left\{-\frac{t^2c_s^2}{2\upsilon_s t}\right\} - \exp\left\{\frac{\left(\frac{r}{c_s}-t\right)^2 c_p^2}{2\upsilon_s t}\right\}\right] + \frac{t}{2}\left[Erf\left(\frac{c_s t}{\sqrt{2\upsilon_s t}}\right) - Erf\left(\frac{\left(t-\frac{r}{c_s}\right)c_s}{\sqrt{2\upsilon_s t}}\right)\right] \tag{14}$$

In the above expressions, $r = \sqrt{x_1^2 + x_2^2 + x_3^2}$, $\gamma = x_1/r$, and $Erf(x) = (2/\pi)\int_0^x e^{-t^2}\,dt$ is the error function. Implied in the above equations is that the acoustic radiation force and resultant tissue displacement are along the same dimension (x_1), namely, the ultrasound beam axis.

Equation (9) is valid for a point-like body force located at the origin $\vec{r} = 0$. Since acoustic radiation forces are complex spatiotemporal patterns, a more suitable analytical expression of the viscoelastic Green's function can be derived using the superposition principle and written as follows [27]:

$$u(\vec{r},t) = \int_{\tau} d\tau \iiint_{v} F(\vec{\varphi},\tau) g(\vec{r}-\vec{\varphi},t-\tau) d\vec{\varphi} \tag{15}$$

where $u(\vec{r},t)$ is the acoustic radiation force-induced displacement field. Solving eqn (15) for a spatiotemporal forcing function describes the displacement fields from acoustic radiation force excitation of propagating shear waves in a viscoelastic soft solid.

2.4. SHEAR WAVE INTERFERENCE PATTERNS

Given two finite amplitude shear waves with equal depth sources separated by distance L, the interference pattern is the superposition of the two waves:

$$U(\vec{R},t) = \sum_{i=1}^{2} u_i(\vec{r}_i,t) \tag{16}$$

where $R = \sqrt{x_1^2 + x_2^2 + x_3^2}$, $r_1 = \sqrt{x_1^2 + (x_2 - L/2)^2 + x_3^2}$ and $r_2 = \sqrt{x_1^2 + (x_2 - L/2)^2 + x_3^2}$. Notation implies that the right (u_1) and left (u_2) propagating shear waves are located at positions $-L/2$ and $+L/2$, respectively. If shear waves are stimulated periodically at low frequency intervals of T_S, then sinusoidal waves can be realized. Since motion is dynamically excited, however, each point location in the image field undergoes periodic oscillations governed by the low frequency transmission of high intensity acoustic radiation force pulses. Assuming the displacement amplitude is proportional to the standard deviation of the sinusoidal wave, computation of the latter produces a surrogate metric of shear wave interference pattern amplitude. Consequently, spatial properties of the shear wave interference patterns can be analyzed to obtain quantitative information about the local shear wave speed and viscosity of the underlying tissue type [29].

3. METHODS

A multiphase simulation was programmed using the software package Matlab (Mathworks, Natick, MA). The general strategy was to analytically compute two-dimensional tissue displacements, due to dynamic acoustic radiation force excitations, using Green's function analysis and then superimpose these displacements onto ultrasound backscattered data fields for each time step of shear wave propagation. Correlation-based speckle tracking techniques allows extraction and visualization of shear wave propagations. Collectively this approach mimics an ultrasound system that both induces and tracks shear wave motion, which is governed by the underlying viscoelastic tissue properties.

The linear acoustic Matlab-based modeling program known as FIELD II [30] independently simulated both high intensity ultrasound pulse transmissions and low intensity backscattered echo fields (i.e., RF lines) describing conventional B-mode imaging. The former induces tissue motion while the latter tracks shear wave propagation across the image plane relative to a reference field. For both configurations described, the transducer was modeled as a 256 element linear array (0.2 mm pitch) with a 5 MHz center frequency.

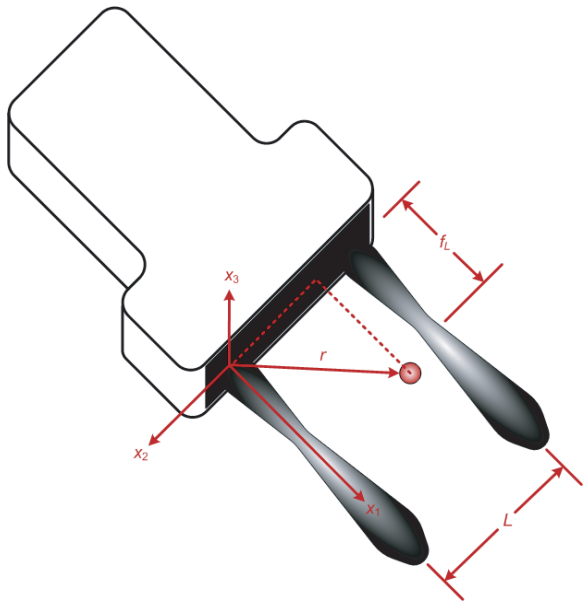

Figure 1 Illustration of ultrasound imaging transducer and vector orientations for a dual beam displacement-inducing configuration with focal depth f_L. Low frequency periodic pulsing of each ultrasound beam (separated by distance L) establish propagating shear waves due to acoustic radiation forces that physically combine to form a shear wave interference pattern. Conventional B-mode imaging sequences track shear wave displacements within the image plane.

As illustrated in Figure 1, a dual beam displacement-inducing transducer configuration was simulated at a focal depth f_L of 15 mm and for a given f-number ($F/\#$) defined as $(F/\#) = f_L/a$ where a is the effective aperture size defined by the number of active elements. Given a 20 μs pulse sequence (100 cycles at 5 MHz), intensities were normalized to a time-average intensity value of 1000 W/cm^2 to reflect relevant radiation force conditions [30]. Subsequently, the combined radiation force distribution from each source was calculated using eqn (1) and used in the viscoelastic Green's function solution of eqn (8) to compute the tissue displacement fields.

Implemented again using FIELD II, a uniform scattering phantom was characterized by isoechoic randomly positioned point targets (250 scatterers per cm^2). These scatterer locations represent initial pre-displacement (reference) positions. Displacements determined via viscoelastic Green's function analysis were used to reposition the scatterers and simulate tissue motion following acoustic radiation force excitation. Specifically, scatterer repositions for each RF line were numerically computed for each time step using shape-preserving piecewise cubic interpolation in direction defined by the beam axis.

For a temporal sequence of ultrasound fields, axial motion was estimated as the peak position of a cross-correlation function applied to congruent pre- and post-displacement RF data segments (60 samples in length). Since these displacement estimates were derived from a discrete valued cross-correlation function, subsample interpolation was employed to improve accuracy [31]. By shifting the data windows, displacement estimates were obtained as a function of depth and repeated until all RF line pairs were processed. Given a temporal

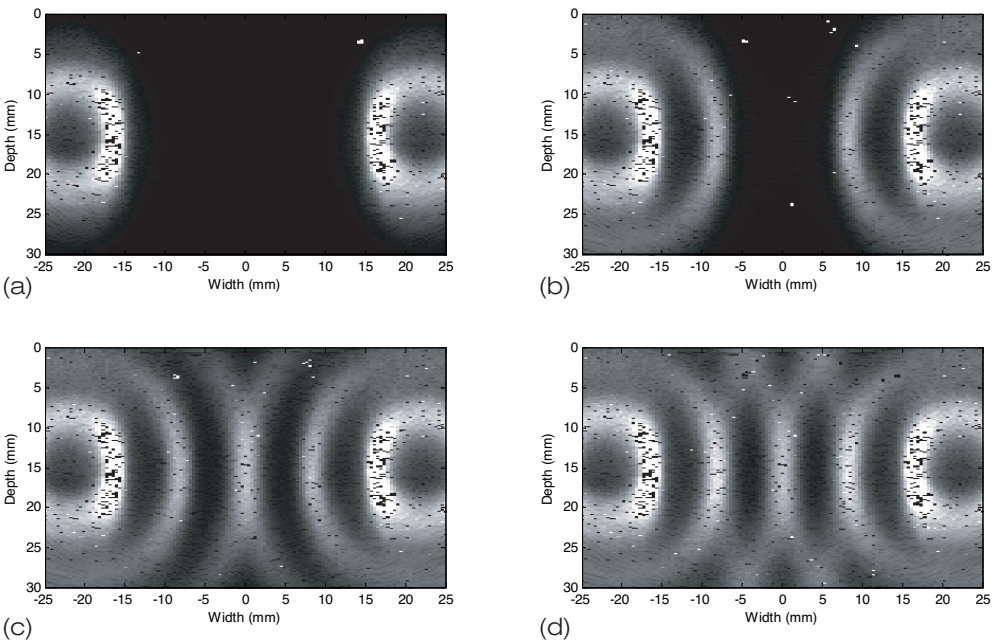

Figure 2 Propagating shear waves (a) 2.0 ms, (b) 4.7 ms, (c) 7.3 ms, and (d) 10.0 ms after acoustic radiation force excitation. For a given source, the distance between shear wave fronts is governed by the product of the high intensity ultrasound beam transmission period (2.5 ms) and tissue shear wave speed (3 m/s).

sequence of images greater than period T_S, the standard deviation at each spatial location was computed and imaged to detail shear wave interference patterns. The above correlation-based processing represents an established technique for extracting tissue motion information from RF fields acquired using B-mode ultrasound imaging.

4. SIMULATIONS

Default simulation parameters are listed in Table 1 unless otherwise noted. Propagating shear waves induced using the simultaneously transmitting dual beam ultrasound configuration is illustrated in Figure 2. For two acoustic radiation force sources located at -22 and 22 mm, respectively, shear waves propagate from the transducer focal zone and gradually attenuate due to wave spreading and viscosity-related dampening. Given a source separation of 44 mm and the values listed in Table 1, the minimal elapsed time before the two propagating shear waves superimpose is 7.3 ms as Figure 2 confirms. Analysis of temporal behavior from a transverse line plot bisecting the two transducer focal zones (Figure 3) reveals that after an elapsed time equal to $(L/2)/c_S$ shear waves superimpose and a periodic standing wave pattern emerges.

For the data presented in Figure 2, computing the standard deviation along the temporal dimension produces a shear wave interference pattern in the far field of both sources (see Figure 4c). Inspection of this image reveals plane wave conditions between the two source focal zones with noticeable beam spreading at higher values of $\vec{R}$. Due to principles of shear wave interference patterns, the spatial period is reduced by a factor of 2 or $\lambda = c_S/2F_S$ denoting the spatial wavelength of the shear wave patterns [17]. As Figure 4 further illustrates, modulating the acoustic radiation force repetition frequency changes the shear

Table 1 Default simulation parameters.

Variable name	Symbol	Value
Beam separation	L	44 mm
Transducer center frequency	F_C	5 MHz
RF Data sampling rate	F_{FAST}	40 MHz
Image frame rate	F_{SLOW}	1500 Hz
Pulse repetition frequency	F_S	400 Hz
Pulse repetition period	T_S	2.5 ms
Lateral *f*-number	$F/\#$	$F/3$
Elevation *f*-number	$F/\#$	$F/2$
Bulk wave speed	c_P	1540 m/s
Shear wave speed	c_S	3.0 m/s
Bulk viscosity	η_P	0.01 Pa s
Shear viscosity	η_S	0.2 Pa s
Tissue mass density	ρ	1000 kg/m^3

wave interference pattern spatial wavelength (i.e., distance between wave fronts) proportionately. An averaged line plot across the images in Figure 4 (from depth of 10 to 20 mm) is presented in Figure 5 for each corresponding F_S. Although shear wave amplitudes are progressively attenuated at distance away from the sources, there is a pronounced interference pattern with a hyperbolic profile. Spatial wavelength measurements and knowledge of F_S permits quantitative estimation of tissue shear wave speed distributions using the above relationship [17].

The influence of the viscoelastic properties of the medium on acoustic radiation force induced shear wave interference patterns was also investigated. Figure 6 shows that as the shear wave speed of the medium increases, the spatial wavelength of the shear wave patterns increases. Wavelength measurements on the spatial line plot in Figure 7 and *a priori* knowledge of the source repetition frequency reveals shear wave speed estimates of 2.6, 3.1, 3.6, and 4.1 m/s compared to the true values of 2.5, 3.0, 3.5, and 4.0 m/s. Collectively, these

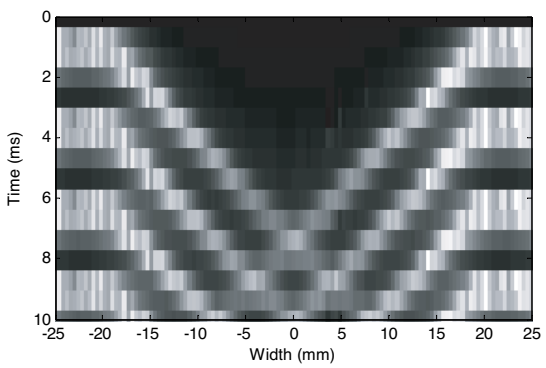

Figure 3 Temporal behavior of a transverse line plot bisecting the two transducer focal zones located at widths of −22 and 22 mm, respectively.

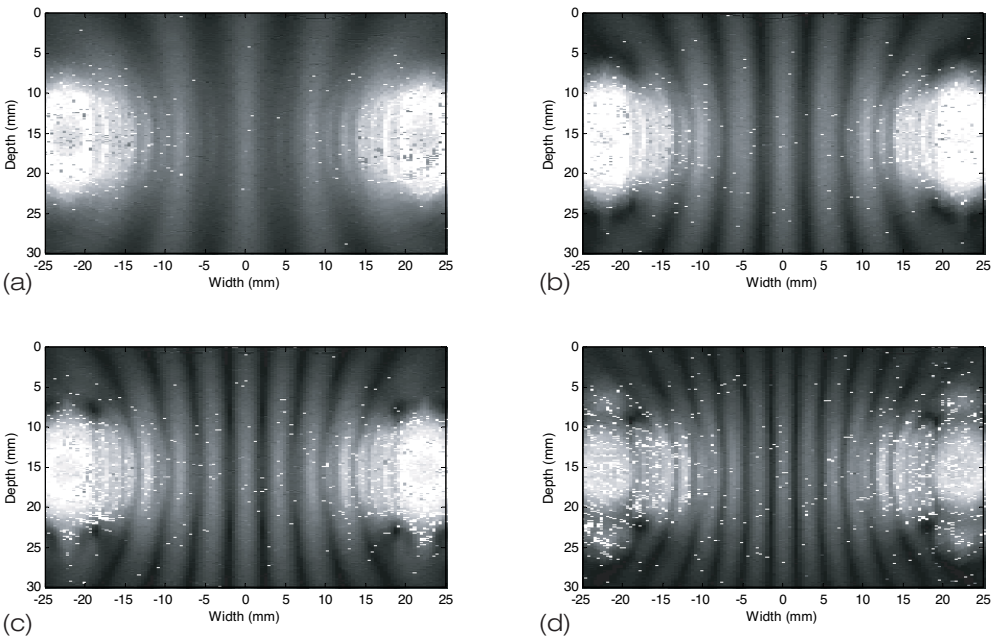

Figure 4 Shear wave interference patterns for acoustic radiation force repetition frequencies of (a) 200 Hz, (b) 300 Hz, (c) 400 Hz, and (d) 500 Hz.

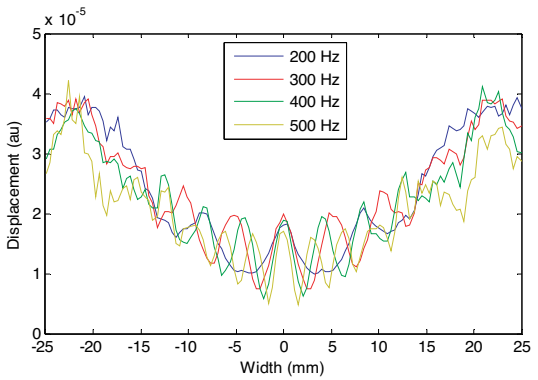

Figure 5 Transverse plots of shear wave interference patterns at a depth equal to the excitation source origin representing acoustic radiation force repetition frequencies from 200 to 500 Hz.

results demonstrate that shear wave interference pattern spatial properties in a far field region bisecting the sources reflect the true viscoelastic properties of the underlying medium.

The shear viscosity component of a viscoelastic medium manifests by attenuating (or dampening) propagating shear waves. This property is observed in Figure 8 which depicts acoustic radiation force induced shear wave interference line plots for a range of shear viscosity values. All else constant, these results detail that increases in the medium shear viscosity progressively attenuates the shear wave interference patterns. This observation establishes a fundamental limit in the ability to generate acceptable signal-to-noise shear

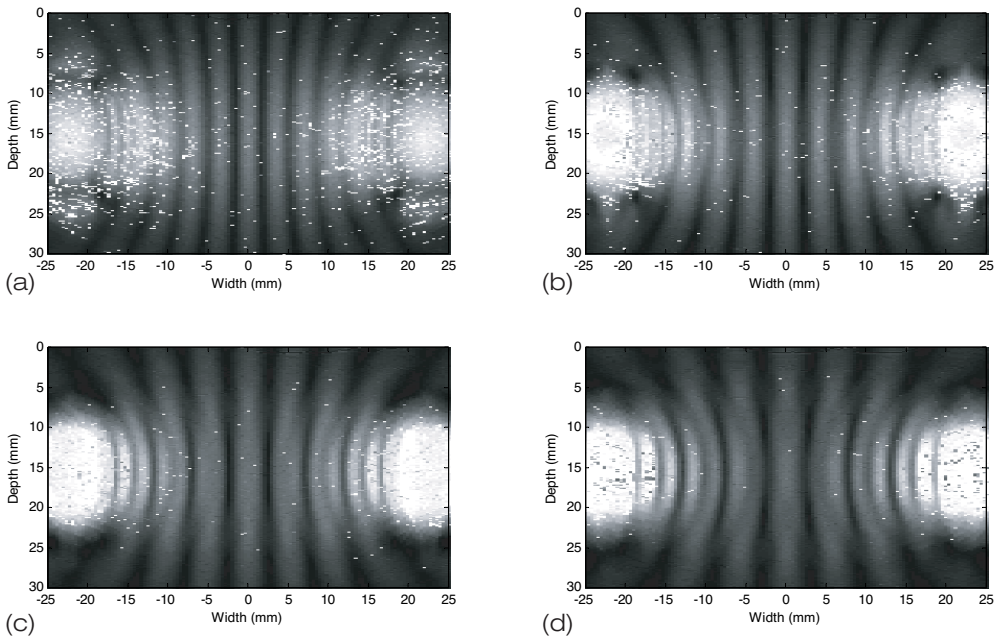

Figure 6 Acoustic radiation force induced shear wave interference patterns in a homogeneous viscoelastic medium characterized by a shear viscosity of 0.2 Pa s and shear wave speeds of (a) 2.5 m/s, (b) 3.0 m/s, (c) 3.5 m/s, and (d) 4.0 m/s.

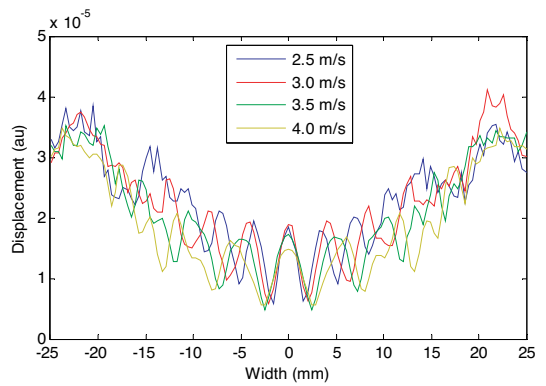

Figure 7 Transverse plots of acoustic radiation force induced shear wave interference patterns in a homogeneous viscoelastic medium characterized by a shear viscosity of 0.2 Pa s and shear wave speeds of 2.5, 3.0, 3.5, or 4.0 m/s.

wave interference patterns in a highly viscous medium and further compound the limitations of shear wave excitation using acoustic radiation forces (e.g., small displacement amplitudes and shear wave propagation and energy dissipation and heating).

Separation distance of equal depth acoustic radiation force origins for a dual beam configuration was evaluated. The summary of results presented in Figure 9 show that as the shear wave sources become progressively closer the number of interference bands diminish

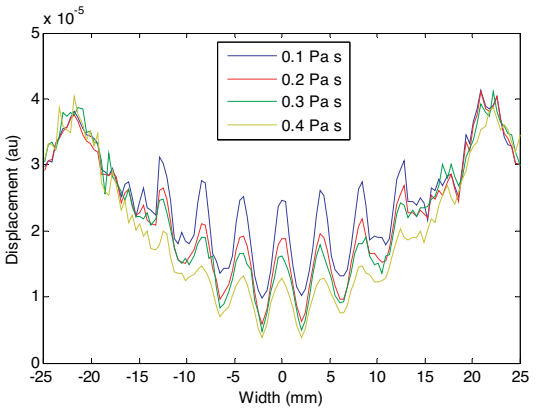

Figure 8 Transverse plots of acoustic radiation force induced shear wave interference patterns in a homogeneous viscoelastic medium characterized by a shear wave speed of 3 m/s and shear viscosity of either 0.1, 0.2, 0.3, or 0.4 Pa s.

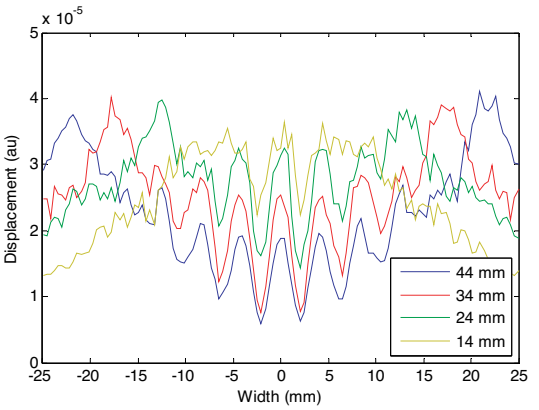

Figure 9 Transverse plots of shear wave interference patterns generated using an acoustic radiation force source pair separation distance of 44, 34, 24, or 14 mm in a homogeneous viscoelastic medium characterized by a shear wave speed of 3 m/s and shear viscosity of 0.2 Pa s.

compromising the ability to extract any useful quantitative viscoelasticity information. To compensate for the lack of spatial information, shear wave generation for the two sources should be excited at higher frequencies or staggered in time. While this latter strategy reduces the available time for displacement tracking, it does afford the opportunity for generating moving shear wave interference patterns [29].

A limitation to shear wave visualization using speckle tracking techniques is the ultrasound imaging frame rate. Sampling theory dictates that the imaging frame rate should be at least two times greater than the shear wave propagation frequency to avoid aliasing. However, since shear waves are stimulated using a short ultrasound pulse, the propagating wave is broadband and knowledge of higher harmonic content is unknown. While these higher harmonic components may be dampened by tissue, determination of an optimal

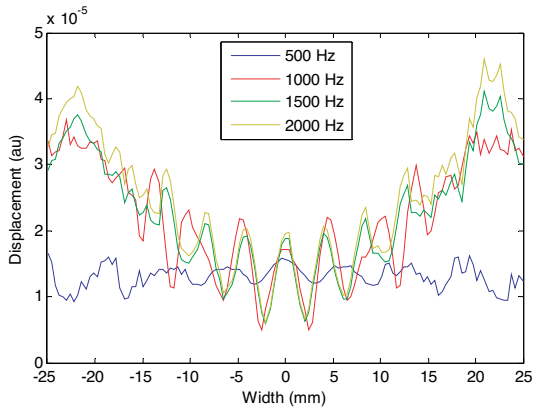

Figure 10 Effect of imaging frame rates on transverse plots of shear wave interference patterns induced using acoustic radiation forces and source repetition frequency of 400 Hz.

sampling frequency is problematic. Notwithstanding, Figure 10 illustrates that shear wave interference patterns induced using an acoustic radiation force repetition frequency of 400 Hz (for both sources) and stepping the image frame rate from 1000 to 2000 Hz progressively improves the interference pattern quality. This is due to increasing the number of temporal images per shear wave oscillation (i.e., higher sampling rate) prior to maximum displacement projection. Conversely, for frame rates below 800 Hz aliasing is observed and shear wave interference patterns do not accurately reflect the viscoelastic properties of the medium. While these high frame rates may be unrealistic for real-time imaging using commercially available ultrasound systems, an alternative to correlation-based speckle tracking is tissue motion estimation using Doppler techniques [33,34] which has been shown to accurately track shear wave motion in real-time [17,18,20,21].

5. CONCLUSIONS

A theoretical formulation of shear wave interference patterns by means of dynamic acoustic radiation forces has been presented. Studied over a spectrum of viscoelastic parameters reflective of both normal and diseased soft tissue, results indicate that acoustic radiation force stimulated shear wave interference patterns may be a useful elasticity imaging modality for tissue characterization and therapy monitoring.

As results indicated, changing the acoustic radiation force repetition frequency changes the shear wave interference pattern spatial wavelength proportionately. However, it was also shown that employing a low repetition frequency can cause excessive delay between propagating shear wave fronts. This situation may seriously complicate viscoelastic parameter estimation since most models assume continuous sinusoidal shear waves. Notwithstanding, above a certain repetition frequency successive shear waves propagating at a given speed will combine to form a sinusoidal pattern (c.f. Figure 4). Unless such repetition frequencies can be indentified for a host of possible tissue types (and varying viscoelastic conditions) beforehand, dynamic shear wave interference pattern stimulation using acoustic radiation forces may need to be optimized for each particular tissue application or consistently stimulated at higher repetition frequencies despite attenuation effects. While not implicitly addressed in this study, displacement tracking must be properly interlaced and

sequenced with the tissue stimulating high intensity ultrasound pulses for the proposed technique to be realized on a commercial ultrasound system.

When utilizing high intensity acoustic radiation forces for tissue stimulation the potential for thermal bioeffects is a concern. While tissue heating due to shear wave stimulation from a single acoustic radiation force pulse is typically less than 0.1^{o} C [35], multiple pulsing strategies can cause temperature rises on the order of several degrees [36]. Creation of a shear wave interference pattern image requires high intensity acoustic radiation force pulses repeatedly delivered to the same tissue regions, therefore, tissue heating is a realistic concern. Shear wave interference images can be theoretically created using only a few repeated pulses so tissue heating may be averted. Regardless, the potential for thermal bioeffects will need to be thoroughly investigated.

Due primarily to attenuation effects, shear wave excitation using external forces limits propagation to superficial or easily accessible tissues. However, shear wave generation using acoustic radiation forces alleviates this limitation and introduces a noninvasive strategy for localized stimulation at depth. Since properly spaced and sequenced dynamic high intensity acoustic radiation force pulses coupled with low intensity ultrasound-based displacement tracking algorithms can induce and image shear wave interference patterns, this novel elasticity imaging method may have clinical utility and warrants further investigation.

ACKNOWLEDGEMENT

The author would like to thank Kevin J Parker at the University of Rochester and Kai Thomenius and Chris Hazard at General Electric Global Research for their insightful comments. This research project was support by NIH grant 5R01AG029804.

REFERENCES

[1] Sarvazyan, A.P., Rudenko, O.V., Swanson, S.D., Fowlkes, J.B. and Emelianov, S.Y., Shear wave elasticity imaging: A new ultrasonic technology of medical diagnostics, *Ultrasound in Medicine and Biology*, 1998, 24, 1419–1435.

[2] Krouskop, T.A., Wheeler, T.M., Kallel, F., Garra, B.S. and Hall, T., Elastic moduli of breast and prostate tissues under compression, *Ultrasonic Imaging*, 1998, 20 260–274.

[3] Sandrin, L., Fourquet, B., Hasquenoph, J.M., Yon, S., Fournier, C., Mal, F., Christidis, C., Ziol, M., Poulet, B., Kazemi, F., Beaugrand, M. and Palau, R., Transient elastography: A new noninvasive method for assessment of hepatic fibrosis, *Ultrasound in Medicine and Biology*, 2003, 29 1705–1713.

[4] Phipps, S., Yang, T.H.J., Habib, F.K., Reuben, R.L., McNeill, S.A., Measurement of tissue mechanical characteristics to distinguish between benign and malignant prostatic disease, *Journal of Urology*, 2005, 66, 447–450.

[5] Zhang, M., Nigwekar, P., Castaneda, B., Hoyt, K., Sant'Agnese, A., Joseph, J.V., Messing, E.M., Rubens, D.J. and Parker, K.J., Quantitative characterization of viscoelastic properties of human prostate correlated with histology, *Ultrasound in Medicine and Biology*, 2007, 34, 1033–1042.

[6] DeLoach, S.S. and Townsend, R.R., Vascular stiffness: Its measurement and significance for epidemiologic and outcome studies, *Clinical Journal of the American Society of Nephrology*, 2008, 3, 184–192.

[7] Hoyt, K., Castaneda, B., Zhang, M., Nigwekar, P., di Sant' Agnese, P.A., Joseph, J.A., Strang, J., Rubens, D.J. and Parker, K.J., Tissue elasticity properties as biomarkers for prostate cancer, *Cancer Biomarkers*, 2008, 4, 213–225.

[8] Hagan, J.J., and Samani, A., Measurement of the hyperelastic properties of 44 pathological ex vivo breast tissue samples, *Physics in Medicine and Biology*, 2009, 54, 2557–2569.

[9] Gao, L., Parker, K.J., Lerner, R.M. and Levinson, S.F., Imaging of the elastic properties of tissue: A review, *Ultrasound in Medicine and Biology*, 1996, 22, 959–977.

[10] Ophir, J., Alam, S.K., Garra, B., Kallel, F., Konofagou, E., Krouskop, T. and Varghese, T. Elastography: Ultrasonic estimation and imaging of the elastic properties of tissues, *Proceedings of the Institution of Mechanical Engineers*, 1999, 213, 203–233.

[11] Greenleaf, J.F., Fatemi, M. and Insana, M., Selected methods for imaging elastic properties of biological tissues, *Annual Review of Biomedical Engineering*, 2003, 5, 57–78.

[12] Walker, W.F., Fernandez, F.J. and Negron, L.A., A method of imaging viscoelastic parameters with acoustic radiation force, *Physics in Medicine and Biology*, 2000, 45, 1437–1447.

[13] Catheline, S., Gennisson, J.L., Delon, G., Fink, M., Sinkus, R., Abouelkaram, S. and Culioli, J., Measurement of viscoelastic properties of homogeneous soft solid using transient elastography: An inverse problem approach, *Journal of the Acoustical Society of America*, 116, 3734–3741.

[14] Chen, S., Fatemi, M. and Greenleaf, J.F., Quantifying elasticity and viscosity from measurement of shear wave speed dispersion, *Journal of the Acoustical Society of America*, 2004, 115, 2781–2785.

[15] McLaughlin, J. and Renzi, D., Shear wave speed recovery in transient elastography and supersonic imaging using propagating fronts, *Inverse Problems*, 2006, 22, 681–706.

[16] Palmeri, M.L., Wang, M.H., Dahl, J.J., Frinkley, K.D. and Nightingale, K.R., Quantifying hepatic shear modulus in vivo using acoustic radiation force, *Ultrasound in Medicine and Biology*, 2008, 34, 546–558.

[17] Wu, Z., Taylor, L.S., Rubens, D.J. and Parker, K.J., Sonoelastographic imaging of interference patterns for estimation of the shear velocity of homogeneous biomaterials, *Physics in Medicine and Biology*, 2004, 49, 911–922.

[18] Wu, Z., Hoyt, K., Rubens, D.J., and Parker, K.J., Sonoelastographic imaging of interference patterns for estimation of shear velocity distribution in biomaterials, *Journal of the Acoustical Society of America*, 2006, 120, 535–545.

[19] McLaughlin, J., Renzi, D., Parker, K. and Wu, Z., Shear wave speed recovery using moving interference patterns obtained in sonoelastography experiments, *Journal of the Acoustical Society of America*, 2007, 121 2438–2446.

[20] Hoyt, K., Parker, K.J. and Rubens, D.J., Real-time shear velocity imaging using sonoelastographic techniques, *Ultrasound in Medicine and Biology*, 2007, 33, 1086–1097.

[21] Hoyt, K., Castaneda, B. and Parker, K.J., Two-dimensional sonoelastographic shear velocity imaging, *Ultrasound in Medicine and Biology*, 2008, 34, 276–288.

[22] Torr, G.R., The acoustic radiation force, *American Journal of Physics*, 1984, 52, 402–408.

[23] Nightingale, K.R., Palmeri, M.L., Nightingale, R.W. and Trahey, G.E., On the feasibility of remote palpation using acoustic radiation force, *Journal of the Acoustical Society of America*, 2001, 110, 625–634.

[24] Landau, L.D. and Lifshitz, E.M., *Theory of elasticity*, Elsevier Butterworth-Heinemann, New York, 1986.

[25] Oestreicher, H.L., Field and impedance of an oscillating sphere in a viscoelastic medium with an application to biophysics, *Journal of the Acoustical Society of America*, 1951, 23, 707–714.

[26] Bercoff, J., Tanter, M. and Fink, M., Supersonic shear imaging: A new technique for soft tissue elasticity mapping, *IEEE Transactions on. Ultrasonics, Ferroelectrics and Frequency Control*, 2004, 51, 396–409.

[27] Bercoff, J., Tanter, M., Muller, M. and Fink, M., The role of viscosity in the impulse diffraction field of elastic waves induced by the acoustic radiation force, *IEEE Transactions on. Ultrasonics, Ferroelectrics and Frequency Control*, 2004, 51, 1523–1536.

[28] Sandrin, L., Cassereau, D. and Fink, M., The role of the coupling term in transient elastography, *Journal of the Acoustical Society of America*, 2004, 115, 73–83.

[29] Hoyt, K., Kneezel, T., Castaneda, B. and Parker, K.J., Quantitative sonoelastography for the in vivo assessment of skeletal muscle viscoelasticity, *Physics in Medicine and Biology*, 2008, 53 4063–4080.

[30] Jensen, J.A. and Svendsen, N.B., Calculation of pressure fields from arbitrarily shaped, apodized, and excited ultrasound transducers, *IEEE Transactions on. Ultrasonics, Ferroelectrics and Frequency Control*, 1992, 39, 262–267.

[31] Palmeri, M.L., Sharma, A.C., Bouchard, R.R., Nightingale, R.W. and Nightingale, K.R., A finite-element method model of soft tissue response to impulsive acoustic radiation force, *IEEE Transactions on. Ultrasonics, Ferroelectrics and Frequency Control*, 2005, 52, 1699–1712.

[32] Céspedes, E.I., Huang, Y., Ophir, J. and Spratt, S., Methods for the estimation of subsample time-delays of digitized echo signals, *Ultrasonic Imaging*, 1995, 17, 142–171.

[33] Huang, S.R., Lerner, R.M., and Parker, K.J., On estimating the amplitude of harmonic vibration from the Doppler spectrum of reflected signals, *Journal of the Acoustical Society of America*, 1990, 88, 2702–2712.

[34] Yamakoshi, Y., Sato, J., and Sato, T., Ultrasonic imaging of internal vibration of soft tissue under forced vibration, *IEEE Transactions on. Ultrasonics, Ferroelectrics and Frequency Control*, 1990, 37, 45–53.

[35] Dahl, J.J., Gianmarco, F.P., Palmeri, M.L., Agrawal, V., Nightingale, K.R. and Trahey, G.E., A parallel tracking method for acoustic radiation force impulse imaging, *IEEE Transactions on. Ultrasonics, Ferroelectrics and Frequency Control*, 2007, 54, 301–312.

[36] Palmeri, M.L. and Nightingale, K.R., On the thermal effects associated with radiation force imaging of soft tissue, *IEEE Transactions on. Ultrasonics, Ferroelectrics and Frequency Control*, 2004, 51, 551–565.